

Article

## Enhanced Photocatalytic Degradation of Methyl Orange Dye under the Daylight Irradiation over CN-TiO<sub>2</sub> Modified with OMS-2

Mohamed Elfatih Hassan, Jing Chen, Guanglong Liu \*, Duanwei Zhu and Jianbo Cai

Laboratory of Eco-Environment Engineering Research, Key Laboratory of Arable Land Conservation, Ministry of Agriculture, College of Resources & Environment, Huazhong Agricultural University, Wuhan 430070, China; E-Mails: mshassan@163.com (M.E.H.); chenjing20122@163.com (J.C.); zhudw@mail.hzau.edu.cn (D.Z.); Jbcai@mail.hzau.edu.cn (J.C.)

\* Author to whom correspondence should be addressed; E-Mail: liugl@mail.hzau.edu.cn; Tel.: +86-27-8728-7184; Fax: +86-27-8739-7735.

External Editor: Klara Hernadi

Received: 22 October 2014; in revised form: 2 December 2014 / Accepted: 9 December 2014 / Published: 12 December 2014

---

**Abstract:** In this study, CN-TiO<sub>2</sub> was modified with cryptomelane octahedral molecular sieves (OMS-2) by the sol-gel method based on the self-assembly technique to enhance its photocatalytic activity under the daylight irradiation. The synthesized samples were characterized by X-ray diffraction (XRD), UV-vis spectroscopy, Fourier transform infrared spectroscopy (FT-IR) and porosimeter analysis. The results showed that the addition of OMS-2 in the sol lead to higher Brunauer-Emmett-Teller (BET) surface area, pore volume, porosity of particle after heat treatment and the specific surface area, porosity, crystallite size and pore size distribution could be controlled by adjusting the calcination temperature. Compared to the CN-TiO<sub>2</sub>-400 sample, CN-TiO<sub>2</sub>/OMS-2-400 exhibited greater red shift in absorption edge of samples in visible region due to the OMS-2 coated. The enhancement of photocatalytic activity of CN-TiO<sub>2</sub>/OMS-2 composite photocatalyst was subsequently evaluated for the degradation of the methyl orange dye under the daylight irradiation in water. The results showed that the methyl orange dye degradation rate reach to 37.8% for the CN-TiO<sub>2</sub>/OMS-2-400 sample under the daylight irradiation for 5 h, which was higher than that of reference sample. The enhancement in daylight photocatalytic activities of the CN-TiO<sub>2</sub>/OMS samples could be attributed to the synergistic effects of OMS-2 coated, larger surface area and red shift in adsorption edge of the prepared sample.

**Keywords:** CN-codoped; OMS-2; daylight; photocatalysis; TiO<sub>2</sub>

---

## 1. Introduction

Today, TiO<sub>2</sub> has been the most widely studied material for the photocatalytic application [1–4]. However, the practical applications of TiO<sub>2</sub> are limited by its large band gap (3.2 eV), which can only active under the UV light irradiation [5–7]. Therefore, several strategies have been developed to shift the optical sensitivity of TiO<sub>2</sub> from UV to the visible-light region for the efficient use of solar energy, such as element doping, metal deposition, surface sensitization, and coupling of composite semiconductors [8]. In element doping, besides traditional single element doping [9], co-doped TiO<sub>2</sub> with two or more elements was confirmed to be an effective way for higher visible light photocatalytic activity. For example, N–F [10,11], N–S [12], B–N [13], and C–N [14–18] co-doped TiO<sub>2</sub> were reported to significantly improve the photocatalytic efficiency under visible light illumination. In our previous paper, carbon and nitrogen co-doped TiO<sub>2</sub> exhibited higher photocatalytic activity than that of reference sample [19]. Unfortunately, nonmetal elements doping can also increase electron-hole recombination rates and lead to an overall decrease in performance despite enhanced light absorption [20].

Combining other semiconductor or support provide a promising way to address this problem. With this approach, the constituents are selected so that efficient charge transfer between them, further to reduce the rate of electron-hole recombination. Examples of composite photocatalysts with improve performance include SnO<sub>2</sub>/TiO<sub>2</sub> [21], ZnO/TiO<sub>2</sub> [22,23], and CdS/TiO<sub>2</sub> [24–26], among others. However, paying attention to the efficient charge transfer, has neglected the effect of specific surface area, which affects the adsorption rate and photocatalytic efficiency because pre-adsorption pollutant molecules on TiO<sub>2</sub> particles facilitate degradation. Therefore, another strategy involves the TiO<sub>2</sub> over support materials with high specific surface area, such as activated carbon, zeolite, silica, and Al<sub>2</sub>O<sub>3</sub> [27–30]. However, the substantial materials decrease photocatalytic activity due to inefficient light harvesting. Thus, the development of new active supports is important for substantial materials to achieve enhanced photocatalytic activity of TiO<sub>2</sub>.

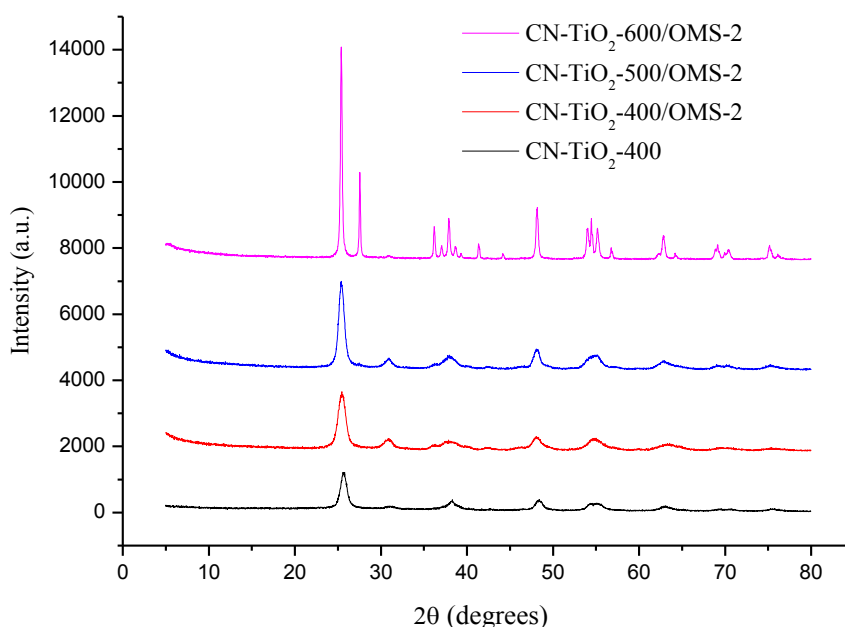
Due to its octahedral molecular sieves structure, high redox potential, and large specific surface area [31], cryptomelane has been reported to have excellent catalytic properties [32], and has been extensively tested in toluene heterogeneous oxidation [33] and 2,4-dichlorophenoxyacetic acid photocatalytic degradation [34]. From our previous work, there should be Mn<sup>4+</sup>/Mn<sup>3+</sup> in the Mn oxide, which could benefit the charge transfer from the TiO<sub>2</sub> to octahedral molecular sieves (OMS-2) [35]. Therefore, in the present study, OMS-2 was employed to modify the CN-TiO<sub>2</sub>, enhance its photocatalytic activity in methyl orange dye degradation under the daylight irradiation and the probable photocatalytic mechanism under daylight irradiation was proposed.

## 2. Results and Discussion

### 2.1. Physical Properties of CN-TiO<sub>2</sub>/OMS-2 and Reference Samples

The XRD patterns of the reference and samples at different calcinations temperatures were shown in Figure 1. Well-defined, broad, diffraction peaks corresponding to the anatase TiO<sub>2</sub> phase were identified for the CN-TiO<sub>2</sub> and CN-TiO<sub>2</sub>/OMS-2-400 sample. However, the rutile TiO<sub>2</sub> phase appeared for the CN-TiO<sub>2</sub>/OMS-2 sample when the calcinations temperature increased to 600 °C. The major peak at 25.3° of anatase is observed in all CN-TiO<sub>2</sub>/OMS-2 samples and this peak became narrow with the calcinations temperature increasing, which pointed to the increase of the TiO<sub>2</sub> crystallite size and crystallinity. The average crystallite size of 16.5, 17.0, 21.8 and 22.9 nm were thus determined by Scherrer formula for the most intense (101) diffraction peak of anatase [36] for CN-TiO<sub>2</sub>/OMS-2-400, CN-TiO<sub>2</sub>/OMS-2-500 and CN-TiO<sub>2</sub>/OMS-2-600, respectively (Table 1). For the CN-TiO<sub>2</sub>/OMS-2 samples, it was found that XRD analysis did not reveal the presence of peaks corresponding to OMS-2 on composite catalysts, as lower concentration of OMS-2 might escape from the detection of XRD, which was similar with other report [37].

**Figure 1.** XRD patterns of as-prepared reference and CN-TiO<sub>2</sub>/OMS-2 nanoparticles calcined at different temperature.



The N<sub>2</sub> adsorption-desorption isotherms and pore size distribution curves of the CN-TiO<sub>2</sub>/OMS-2 samples calcined at different temperature are shown in Figure 2. The pore size distribution was calculated from the desorption branch of nitrogen isotherms by barret-joyner-Halenda (BJH) method using the Halsey equation. It can be seen that the N<sub>2</sub> adsorption-desorption isotherms of CN-TiO<sub>2</sub>/OMS-2 samples vary with increasing calcination temperature as shown in Figure 2a. The CN-TiO<sub>2</sub>/OMS-2 with different calcination temperature shows the significant hysteresis loop in the adsorption-desorption isotherms, which indicates that the synthesized CN-codoped TiO<sub>2</sub> samples are typical mesoporous materials [38]. The pore size distribution of the resulting samples showed considerable difference as displayed in Figure 2b. All samples showed unimodal pore size distribution

and the pore size distribution of CN-TiO<sub>2</sub>/OMS-2-400 was very narrow implying good homogeneity of the pores. With increasing of calcination temperature, the pore size distribution of samples became broad, which due to sintering and growth of crystallites, though the material retained its highly porous characteristics [39]. With increasing of calcination temperature, the bigger crystallites aggregation could form bigger pores. Therefore, the diameter of pore became bigger while the volume of pore became smaller with increasing calcination temperature [40]. The Brunauer-Emmett-Teller (BET) specific surface areas of CN-TiO<sub>2</sub>/OMS-2-400 sample and reference material (calcinations at 400 °C) are recorded at 114.7 m<sup>2</sup>·g<sup>-1</sup> and 40.1 m<sup>2</sup>·g<sup>-1</sup> (summarized in Table 1), respectively. The mesoporous structure and high BET surface area of CN-TiO<sub>2</sub>/OMS-2 are expected to enhance adsorption of organic compounds onto the particle surface. It is noteworthy that the loading of OMS-2 on the TiO<sub>2</sub> particles has greatly increased the specific area of the material. This phenomenon can be attributed to the presence of the OMS-2, which acts as a dispersing template to downsize the TiO<sub>2</sub> nanostructures during the synthesis process. Therefore, the adsorption capacity and photocatalytic activity of the synthesized particles could be enhanced since adsorption processes are predominantly driven by surface reaction on the materials.

**Table 1.** Structural characteristics of CN-TiO<sub>2</sub>/OMS-2 with calcination temperature and reference material.

Samples	$S_{BET}(m^2 \cdot g^{-1})^a$	Pore volume (cm <sup>3</sup> ·g <sup>-1</sup> )	Crystal phase	Crystal size (nm) <sup>b</sup>
CN-TiO <sub>2</sub> -400	40.1	0.074	Anatase	16.5
CN-TiO <sub>2</sub> /OMS-2-400	114.7	0.252	Anatase	17.0
CN-TiO <sub>2</sub> /OMS-2-500	79.5	0.278	Anatase	21.8
CN-TiO <sub>2</sub> /OMS-2-600	21.9	0.187	Anatase+Rutile	22.9

a. Determined by N<sub>2</sub> porosimetry by converting the adsorbed gas amount to liquid volume at the relative pressure of 0.99; b. Based on XRD using Scherrer Formula  $D = 0.9\lambda/(B \times \cos\theta)$ , where  $\lambda = 0.154$  nm and  $B$  = full width at half maximum (FWHM) of the highest peak.

**Figure 2.** (a) Nitrogen adsorption-desorption isotherms and (b) pore size distribution of CN-TiO<sub>2</sub>/OMS-2 samples with different calcination temperature.

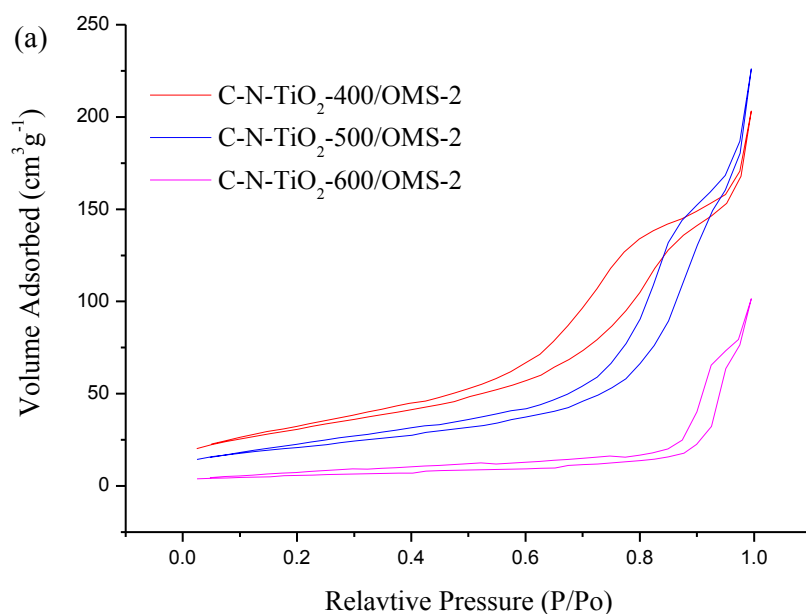
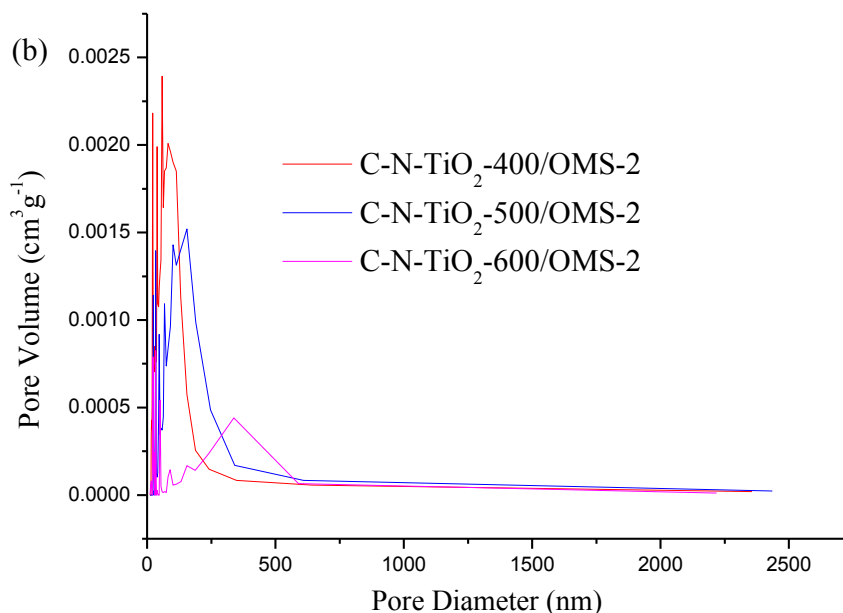
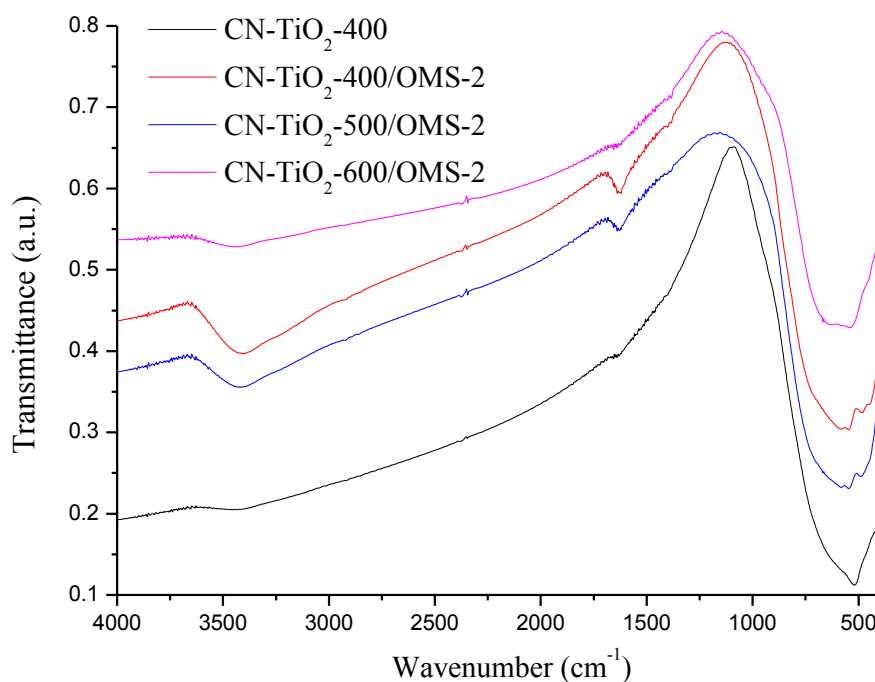
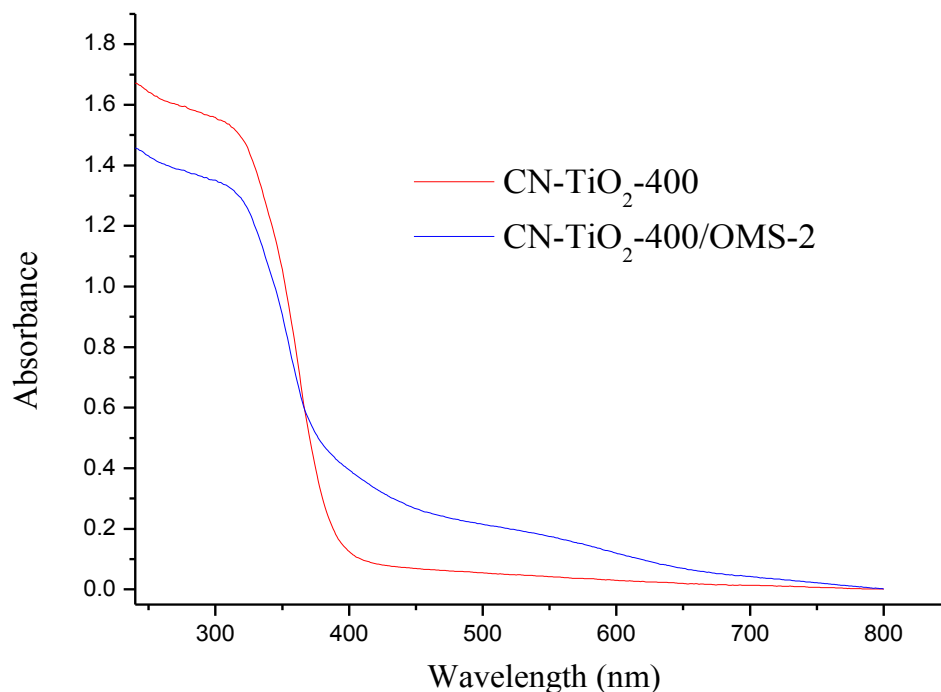


Figure 2. Cont.



To give additional evidence and further to confirm the doping of OMS-2, Fourier transform infrared spectroscopy (FT-IR) characterizations were performed. The infrared spectroscopy of CN-TiO<sub>2</sub>/OMS-2 samples and reference material are presented in Figure 3. The characteristic IR absorption peaks at 3136, 2330, 1640, 1400 and 530 cm<sup>-1</sup> were observed in all samples. The bands at 1640 cm<sup>-1</sup> and the wide bands at 3136 cm<sup>-1</sup> are resultant from O–H bending of adsorbed water molecules, which has been reported that OH bonded group on the catalyst surface could benefit the photocatalysis efficiency of TiO<sub>2</sub> materials. It noteworthy that the intensity of OH bonded group in CN-TiO<sub>2</sub>/OMS-2 was stronger than that of reference sample, which may be due to the OH bonded group in the doped OMS-2. This would enhance the photocatalytic activity of CN-TiO<sub>2</sub>/OMS-2 sample. The bands at 2330 cm<sup>-1</sup> are assigned to the stretching vibrations of the C=O bonds, which should be attributed to the T80 used in the sol. The bands at 1400 cm<sup>-1</sup> are assigned to the stretching vibrations of the N–H bonds in NH<sub>3</sub>, which evidences the presence of NH<sub>3</sub> in Ti complex [16,17]. The NH<sub>3</sub> in the Ti complex is regarded as nitrogen source for the N-doped TiO<sub>2</sub>. With the calcination temperature increasing, the N–H bands at 1400 cm<sup>-1</sup> disappear, which evidences the decomposition of NH<sub>3</sub>. The characteristic IR absorption peaks at 530 and 470 cm<sup>-1</sup> are spectral features of OMS-2. Compared with the IR absorption spectrum of the CN-TiO<sub>2</sub>/OMS-2-400 and reference sample, it shows both the characteristic IR absorption of CN-TiO<sub>2</sub>/OMS-2-400 and that of the reference sample around 530 cm<sup>-1</sup>. It proved that the synthesized powder was the composite of OMS-2 and CN-TiO<sub>2</sub>.

Figure 4a shows the UV-vis absorption spectra of the CN-TiO<sub>2</sub>/OMS-2-400 and reference samples. It has been reported that pure TiO<sub>2</sub> only absorbed ultraviolet radiation of less than 400 nm. Due to the carbon and nitrogen co-doping, the reference sample showed obvious absorption in the visible light region of 400–700 nm. Compared to the reference sample, the CN-TiO<sub>2</sub>/OMS-2-400 exhibited stronger absorption in the visible light region. It indicated that the presence of carbon and nitrogen co-doping or synergistic effect between OMS-2 and TiO<sub>2</sub> support that aid the photocatalytic activity in the visible-light region. In the present study, OMS-2 may interact with TiO<sub>2</sub> and CN-codoping also increased the visible light absorption ability of the composite.

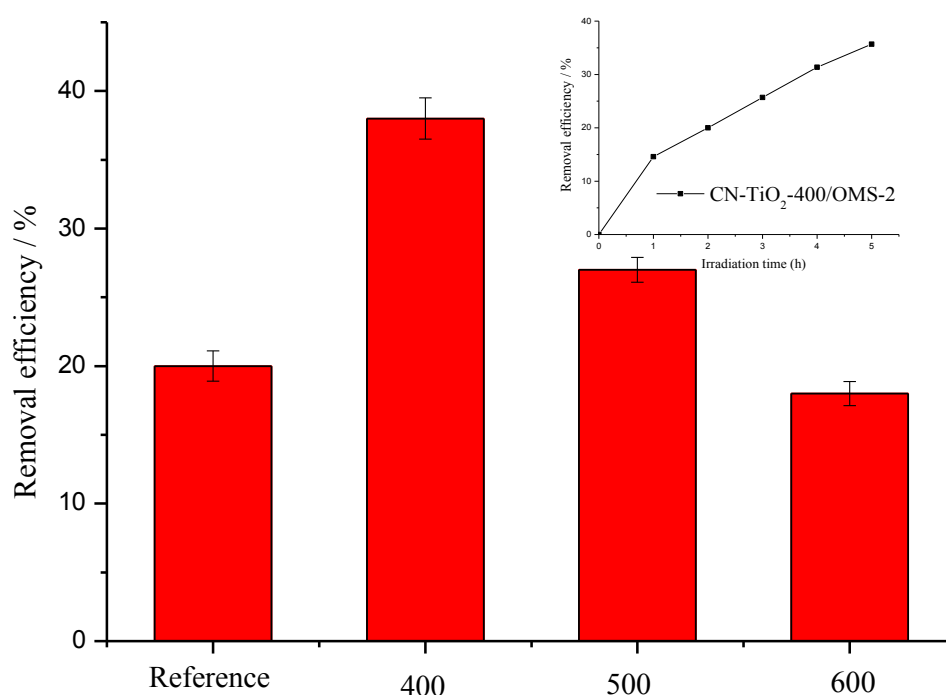
**Figure 3.** FT-IR spectra of CN-TiO<sub>2</sub>/OMS-2 samples and reference.**Figure 4.** Optical properties of CN-codoped TiO<sub>2</sub>/OMS-2 sample compared to reference.

## 2.2. Photocatalytic Activity of CN-TiO<sub>2</sub>/OMS-2 Samples

Figure 5 shows the photocatalytic degradation of methyl orange dye by the CN-TiO<sub>2</sub>/OMS-2 samples with various calcination temperature and reference sample under the daylight irradiation. It can be seen that the 20% methyl orange dye was degraded by the reference sample, which should be contributed to the C and N co-doped on the TiO<sub>2</sub>. When the CN-TiO<sub>2</sub>/OMS-2 samples were added, the methyl orange dye degradation rate increased and CN-TiO<sub>2</sub>/OMS-2-400 exhibited highest

photocatalytic activity in the methyl orange dye degradation under the daylight irradiation. However, the removal efficiencies steadily decreased with the calcination temperature increased. This result further confirmed that the sample calcined at 400 °C possessed the highest photocatalytic activity. From our results, the photocatalytic activity of samples was extremely related with the heat treatment, which were agreement with other reports. For the CN-TiO<sub>2</sub>/OMS-2 sample, the photocatalytic activity of samples decreased with the calcination temperature increase, which may be due to the C and N removed in the higher temperature. This will reduce the e<sup>-</sup> and h<sup>+</sup> generated on the surface of samples, further reducing the photocatalytic activity of samples.

**Figure 5.** The dependence of the removal efficiency ( $R$  (%)) of photocatalytic oxidation of methyl orange under daylight irradiation on calcination temperature (Insertion is methyl degradation by CN-TiO<sub>2</sub>/OMS-2).

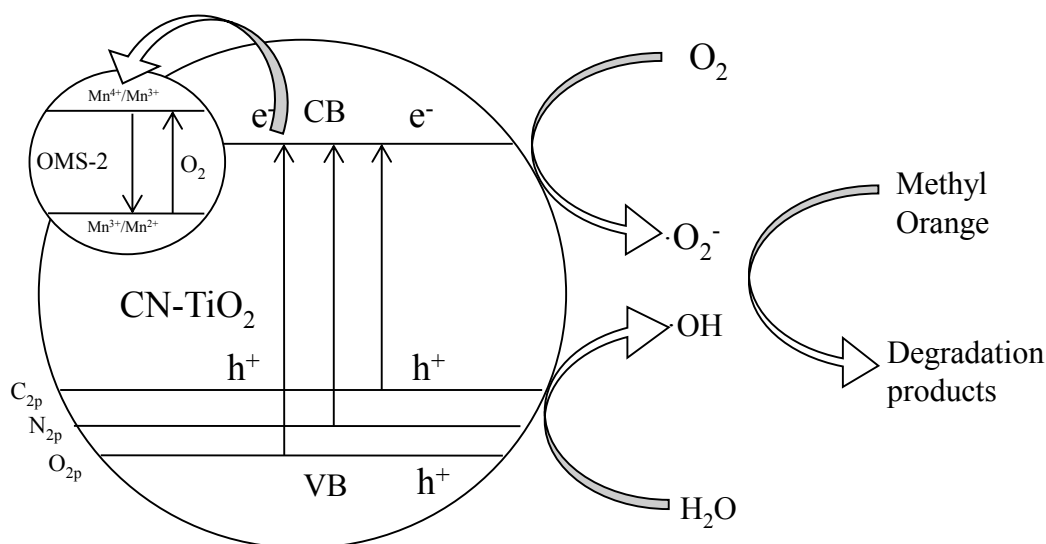


### 2.3. Photocatalytic Mechanism

The band structure of bare CN-TiO<sub>2</sub>/OMS-2 is shown in Figure 6. The O 2p orbitals contribute to make up a valence band (VB) while Ti 3d contributes for a conduction band (CB). Since the distance between VB (O 2p) and CB (Ti 3d) of pure TiO<sub>2</sub> is large (3.31 eV) (Figure 6), absorption of visible-light is negligible and hence TiO<sub>2</sub> showed low photocatalytic activity in the degradation of methyl orange. On the other hand, the new absorption band appeared below the conduction band edge of TiO<sub>2</sub> in CN-TiO<sub>2</sub> (Figure 6) due to C and N doped is responsible for visible light absorption in CN-TiO<sub>2</sub>. For the CN-TiO<sub>2</sub>/OMS-2 samples, the OMS-2 nanoparticle was coated on the surface of CN-TiO<sub>2</sub> support. It has been reported that Mn<sup>4+</sup>/Mn<sup>3+</sup> existed in the Mn oxide due to the average oxidation state (AOS) of 3.75 in OMS-2, which could benefit the charge transfer from the TiO<sub>2</sub> to OMS-2 [35]. When visible-light was illuminated on CN-TiO<sub>2</sub>/OMS-2, the electrons excited from the valence band to conduction band leaving holes in the valence band of TiO<sub>2</sub>. The excited electrons in the conduction band are transferred to Mn<sup>4+</sup>/Mn<sup>3+</sup> resulting the reduction of Mn<sup>4+</sup>/Mn<sup>3+</sup> to Mn<sup>3+</sup>/Mn<sup>2+</sup>.

Hence the holes with strong oxidation power generated in the VB of CN-TiO<sub>2</sub>/OMS-2 and the electrons in the conduction band are effectively separated upon visible-light irradiation. This circulatory system will inhibit the electron-hole recombination, increase the generated rate of •OH, and improve the photocatalytic activity. For the methyl orange dye degradation, the dye could transfer to the excited state of dye under the light irradiation, which rapidly reacted with •OH and resulted in the degradation [41].

**Figure 6.** Possible mechanism for the photocatalytic activity of CN-TiO<sub>2</sub>/OMS-2 samples to methyl orange degradation.



### 3. Experimental Section

#### 3.1. Chemicals

T80 (Guoyao Chemical Co., Shanghai, China), isopropyl alcohol (i-PrOH, 99.8%, Guoyao Chemical Co.), titanium tetraisopropoxide (TTIP, 97%, Sigma-Aldrich, St. Louis, MO, USA), acetic acid (AcOH, Guoyao Chemical Co., Shanghai, China), HNO<sub>3</sub> (Sinopharm Chemical Reagent Co., Shanghai, China), and methyl orange (Sinopharm Chemical Reagent Co., Shanghai, China) were used as received.

#### 3.2. Synthesis of Daylight-Activated CN-TiO<sub>2</sub>/OMS-2 Samples

CN-TiO<sub>2</sub>/OMS-2 sample was prepared by the self-assembly surfactant-based sol-gel method under mild conditions as follow. A nonionic surfactant T80 was employed as the pore directing agent and carbon precursor in the modified sol-gel solution. T80 (4 g) was dissolved in isopropanol (20 mL) and then acetic acid (3 mL) was added for the *in-situ* formation of water. Before adding the Ti precursor, anhydrous ethylenediamine (3 mL) was induced in the solution as a nitrogen source. Then, titanium (IV) isopropoxide (6 mL) was added dropwise under vigorous stirring, and 20 mL acetic acid was added. The transparent, homogeneous and stable solution was obtained after stirring 24 h at room temperature. Then, 0.0468 g OMS-2 prepared as Liu *et al.* [35] reported was added to the solution and aged at room temperature for 10 h. To synthesize particles, the solution was dried at 120 °C for 6 h and



then calcined at 400, 500 and 600 °C for 3 h. For comparison, CN-TiO<sub>2</sub> and TiO<sub>2</sub> samples were prepared through the same method, without adding the corresponding dopants and calcined at 400 °C for 3 h.

### 3.3. Characterization of Synthesized CN-TiO<sub>2</sub>/OMS-2 Samples

To study the crystal structure and crystallinity of the CN-TiO<sub>2</sub>/OMS-2 and reference samples, X-ray diffraction (XRD) analysis was performed on X'Pert PRO (D8 Advance, Bruker Co., Bremen, Germany) using Cu K $\alpha$  ( $\lambda = 1.5406 \text{ \AA}$ ) radiation. The Brunauer-Emmett-Teller (BET) surface area, pore volume, porosity, Barret-Joyner-Halenda (BJH) pore size and distribution (based on nitrogen adsorption and desorption isotherms) were determined by Tristar 300 (Micromeritics, Micromeritics Instrument Corporation, Norcross, GA, USA) porosimeter analyzer. All the test powders were collected from the films and purged with nitrogen gas for 2 h at 150 °C using Flow prep 060 (Micromeritics). Fourier transform infrared (FT-IR) spectroscopy was carried out using Thermo Scientific Nicolet 6700 spectrometer (Waltham, MA, USA) to detect the presence of carbon group on the samples. Measurement range was 4000–400 cm<sup>-1</sup>, with a 4 cm<sup>-1</sup> resolution, 0.475 cm<sup>-1</sup>/s scan speed and 32 scans. The technique applied was attenuated total reflectance (ATR) with an Avantar multibounce HATR accessory with ZnSe crystal at 45°. To investigate the light absorption and optical band gap of the synthesized TiO<sub>2</sub> nanoparticles, the UV-vis absorption spectra were obtained with a UV-vis spectrophotometer (UV-2450 PC, Shimadzu Co., Kyoto, Japan) mounted with an integrating sphere accessory (ISR1200) using BaSO<sub>4</sub> as reference standard.

### 3.4. Photocatalytic Evaluation with Methyl orange under Daylight

After synthesis and characterization, photocatalytic activity of CN-TiO<sub>2</sub>/OMS-2 samples were evaluated by the degradation of methyl orange dye under simulated daylight using two fluorescent lamps (20W, Shanghai Yaming Co. Ltd., Shanghai, China) as light source and the light intensity on the surface of reactor was 2 mW/cm<sup>2</sup> measured using a UV intensity meter (UV-I, Beijing Shida Ltd., Beijing, China). Methyl orange is a pH indicator and was examined in the red form. To this end, the pH of the sample was adjusted with nitric acid to acidic condition. The degradation rate of the dyes was monitored by recording the variations of the particular absorption-band maximum ( $\lambda_{\text{max}} = 517 \text{ nm}$ , as seen in Figure S1) in the absorbance spectrum using a UV2450 UV-vis spectroscopy. (Shimadzu, Kyoto, Japan). Before each experiment, a particles suspension (0.5 g/L) solution was prepared and dispersed using an ultrasonicator (2510R-DH, Branson, Beijing, China) for 24 h. 10 mL methyl orange solution (500 mg/L) was transferred to a 50 mL particles suspension placed in reactor to achieve an initial concentration of 100 mg/L. Finally, 50  $\mu\text{L}$  HNO<sub>3</sub> (0.05 mol·L<sup>-1</sup>) was added into the solution. During the irradiation, the reactor was sealed with parafilm and continuously mixed to minimize mass transfer limitations. A 2 mL sample was withdrawn at time 0, 1, 2, 3, 4 and 5 h. The photocatalyst was immediately removed from the samples after centrifugation and the concentration of methyl orange dye in the samples was determined by UV-vis spectroscopy.

#### 4. Conclusions

The daylight-active carbon and nitrogen co-doped TiO<sub>2</sub> combined with OMS-2 was successfully synthesized by the sol-gel method based on the self-assembly technique. The CN-TiO<sub>2</sub>/OMS-2 samples exhibited larger surface area, pore volume and porosity of particle than that of sample without of OMS-2 adding. It was also found that the specific surface area, porosity, crystallite size and pore size distribution of TiO<sub>2</sub>/OMS-2 samples could be controlled by adjusting the calcination temperature. The TiO<sub>2</sub>/OMS-2-400 sample exhibited the highest photocatalytic activity during the degradation of methyl orange dye among samples calcined at other temperature and reference sample under the daylight irradiation. The enhanced daylight activity of TiO<sub>2</sub>/OMS-2 could be attributed to the OMS-2 doping, synergistic effects of carbon, nitrogen and OMS-2 doping, large surface area, good crystallization and red shift in adsorption edge of the prepared sample.

#### Supplementary Materials

Supplementary materials can be accessed at: <http://www.mdpi.com/1996-1944/7/12/8024/s1>.

#### Acknowledgments

This research was financially supported by the National Natural Science Foundation of China (41401547), Natural Science Foundation of Hubei Province of China (2014CFB283), Fundamental Research Funds for the Central Universities (2013QC044), and Major Science and Technology Program for Water Pollution Control and Treatment (2012ZX07104-001).

#### Author Contributions

Mohamed Elfatih Hassan designed the experiments, and edited the paper. Jing Chen carried out the experiments. Guanglong Liu directed, carried out the experiments and wrote the paper. Duanwei Zhu and Jianbo Cai advised about the scientific meanings of this study and edited the paper.

#### Conflicts of Interest

The authors declare no conflict of interest.

#### References

1. Akhavan, O.; Azimirad, R. Photocatalytic property of Fe<sub>2</sub>O<sub>3</sub> nanograin chains coated by TiO<sub>2</sub> nanolayer in visible light irradiation. *Appl. Catal. A Gen.* **2009**, *369*, 77–82.
2. Liu, S.; Yu, J.; Jaroniec, M. Tunable photocatalytic selectivity of hollow TiO<sub>2</sub> microspheres composed of anatase polyhedra with exposed {001} facets. *J. Am. Chem. Soc.* **2010**, *132*, 11914–11916.
3. Xiang, Q.J.; Yu, J.G.; Jaroniec, M. Graphene-based semiconductor photocatalysts. *Chem. Soc. Rev.* **2012**, *41*, 782–796.

4. Devi, L.G.; Kottam, N.; Kumar, S.G. Preparation and characterization of Mn-doped titanates with a bicrystalline framework: Correlation of the crystallite size with the synergistic effect on the photocatalytic activity. *J. Phys. Chem. C* **2009**, *113*, 15593–15601.
5. Wen, C.Z.; Jiang, H.B.; Qiao, S.Z.; Yang, H.G.; Lu, G.Q. Synthesis of high-reactive facets dominated anatase TiO<sub>2</sub>. *J. Mater. Chem.* **2011**, *21*, 7052–7061.
6. Xiang, Q.J.; Yu, J.G.; Wang, W.G.; Jaroniec, M. Nitrogen self-doped nanosized TiO<sub>2</sub> sheets with exposed {001} facets for enhanced visible-light photocatalytic activity. *Chem. Commun.* **2011**, *47*, 6906–6908.
7. Yu, J.G.; Xiang, Q.J.; Zhou, M.H. Preparation, characterization and visible-light-driven photocatalytic activity of Fe-doped titania nanorods and first principles study for electronic structures. *Appl. Catal. B Environ.* **2009**, *90*, 595–602.
8. Zhan, S.; Yang, Y.; Gao, X.; Yu, H.; Yang, S.; Zhu, D.; Li, Y. Rapid degradation of toxic toluene using novel mesoporous SiO<sub>2</sub> doped TiO<sub>2</sub> nanofibers. *Catal. Today* **2014**, *225*, 10–17.
9. Yang, X.; Cao, C.; Erickson, L.; Hohn, K.; Maghirang, R.; Klabunde, K. Photo-catalytic degradation of Rhodamine B on C-, S-, N-, and Fe-doped TiO<sub>2</sub> under visible-light irradiation. *Appl. Catal. B Environ.* **2009**, *91*, 657–662.
10. Giannakas, A.E.; Seristatidou, E.; Deligiannakis, Y.; Konstantinou, I. Photocatalytic activity of N-doped and N–F co-doped TiO<sub>2</sub> and reduction of chromium (VI) in aqueous solution: An EPR study. *Appl. Catal. B Environ.* **2013**, *132*, 460–468.
11. Wang, W.; Ni, Y.; Lu, C.; Xu, Z. Hydrogenation Temperature related inner structures and visible-light-driven photocatalysis of N–F co-doped TiO<sub>2</sub> nanosheets. *Appl. Surf. Sci.* **2014**, *290*, 125–130.
12. Yu, J.; Zhou, M.; Cheng, B.; Zhao, X.; Mol, J. Preparation, characterization and photocatalytic activity of *in situ* N,S-codoped TiO<sub>2</sub> powders. *Catal. A Chem.* **2006**, *246*, 176–184.
13. Zhang, K.; Wang, X.; He, T.; Guo, X.; Feng, Y. Preparation and photocatalytic activity of B–N co-doped mesoporous TiO<sub>2</sub>. *Powder Technol.* **2014**, *253*, 608–613.
14. Xu, Q.C.; Wellia, D.V.; Yan, S.; Liao, D.W.; Lim, T.M.; Tan, T.T.Y. Enhanced photocatalytic activity of C–N-codoped TiO<sub>2</sub> films prepared via an organic-free approach. *J. Hazard. Mater.* **2011**, *188*, 172–180.
15. Xu, Q.C.; Wellia, D.V.; Sk, M.A.; Lim, K.H.; Loo, J.S.C.; Liao, D.W.; Amal, R.; Tan, T.T.Y. Transparent visible light activated C–N–F-codoped TiO<sub>2</sub> films for self-cleaning applications. *J. Photochem. Photobiol. A Chem.* **2010**, *210*, 181–187.
16. Wang, X.; Lim, T. Solvothermal synthesis of C–N codoped TiO<sub>2</sub> and photocatalytic evaluation for bisphenol A degradation using a visible-light irradiated LED photoreactor. *Appl. Catal. B Environ.* **2010**, *100*, 355–364.
17. Wang, X.; Lim, T. Effect of hexamethylenetetramine on the visible-light photocatalytic activity of C–N codoped TiO<sub>2</sub> for bisphenol A degradation: evaluation of photocatalytic mechanism and solution toxicity. *Appl. Catal. A Gen.* **2011**, *399*, 233–241.
18. Kakroudi, M.A.; Kazemi, F.; Kaboudin, B. Highly efficient photodeoximation under green and blue LEDs catalyzed by mesoporous C–N codoped nano TiO<sub>2</sub>. *J. Mol. Catal. A Chem.* **2014**, *392*, 112–119.

19. Liu, G.; Han, C.; Pelaez, M.; Zhu, D.; Liao, S.; Likodimos, V.; Kontos, A.G.; Falaras, P.; Dionysiou, D.D. Enhanced visible light photocatalytic activity of C–N-codoped TiO<sub>2</sub> films for the degradation of microcystin-LR. *J. Mol. Catal. A Chem.* **2013**, *373*, 58–65.
20. Xu, L.; Steinmiller, M.P.; Skrabalak, S.E. Achieving synergy with a potential photocatalytic Z-scheme: Synthesis and evaluation of nitrogen-doped TiO<sub>2</sub>/SnO<sub>2</sub> composites. *J. Phys. Chem. C* **2012**, *116*, 871–877.
21. Jaiswal, M.K.; Kumar, R.; Kanjilal, D. Dense electronic excitation induced modification in TiO<sub>2</sub> doped SnO<sub>2</sub> nanocomposite films. *J. Alloy. Compd.* **2014**, *610*, 651–658.
22. Wang, Y.; Zhu, S.; Chen, X.; Tang, Y.; Jiang, Y.; Peng, Z.; Wang, H. One-step template-free fabrication of mesoporous ZnO/TiO<sub>2</sub> hollow microspheres with enhanced photocatalytic activity. *Appl. Surf. Sci.* **2014**, *307*, 263–271.
23. Pozan, G.S.; Kambur, A. Significant enhancement of photocatalytic activity over bifunctional ZnO–TiO<sub>2</sub> catalysts for 4-chlorophenol degradation. *Chemosphere* **2014**, *105*, 152–159.
24. Li, L.; Wang, L.; Hu, T.; Zhang, W.; Zhang, X.; Chen, X. Preparation of highly photocatalytic active CdS/TiO<sub>2</sub> nanocomposites by combining chemical bath deposition and microwave-assisted hydrothermal synthesis. *J. Solid State Chem.* **2014**, *218*, 81–89.
25. Guo, X.; Chen, C.; Song, W.; Wang, X.; Di, W.; Qin, W. CdS embedded TiO<sub>2</sub> hybrid nanospheres for visible light photocatalysis. *J. Mol. Catal. A Chem.* **2014**, *387*, 1–6.
26. Song, G.; Xin, F.; Chen, J.; Yin, X. Photocatalytic reduction of CO<sub>2</sub> in cyclohexanol on CdS–TiO<sub>2</sub> heterostructured photocatalyst. *Appl. Catal. A Gen.* **2014**, *473*, 90–95.
27. Murgolo, S.; Petronella, F.; Ciannarella, R.; Comparelli, R.; Agostiano, A.; Curri, M.L.; Mascolo, G. UV and solar-based photocatalytic degradation of organic pollutants by nano-sized TiO<sub>2</sub> grown on carbon nanotubes. *Catal. Today* **2015**, *240*, 114–124.
28. Pang, D.; Wang, Y.; Ma, X.; Ouyang, F. Fluorine promoted and silica supported TiO<sub>2</sub> for photocatalytic decomposition of acrylonitrile under simulant solar light irradiation. *Chem. Eng. J.* **2014**, *258*, 43–50.
29. Polat, M.; Soylu, A.M.; Erdogan, D.A.; Erguven, H.; Vovk, E.I.; Ozensoy, E. Influence of the sol–gel preparation method on the photocatalytic NO oxidation performance of TiO<sub>2</sub>/Al<sub>2</sub>O<sub>3</sub> binary oxides. *Catal. Today* **2015**, *241*, 25–32.
30. Pan, Z.; Stemmler, E.A.; Cho, H.J.; Fan, W.; LeBlanc, L.A.; Patterson, H.H.; Amirbahman, A. Photocatalytic degradation of 17 $\alpha$ -ethinylestradiol (EE2) in the presence of TiO<sub>2</sub>-doped zeolite. *J. Hazard. Mater.* **2014**, *279*, 17–25.
31. Suib, S.L. Sorption, catalysis, separation design. *Chem. Innovat.* **2000**, *30*, 27–33.
32. Suib, S.L. Structure, porosity, and redox in porous manganese oxide octahedral layer and molecular sieve materials. *J. Mater. Chem.* **2008**, *18*, 1623–1631.
33. Abecassis-Wolfovich, M.; Jothiramalingam, R.; Landau, M.V.; Herskowitz, M.; Viswanathan, B.; Varadarajan, T.K. Cerium incorporated ordered manganese oxide OMS-2 materials: Improved catalysts for wet oxidation of phenol compounds. *Appl. Catal. B Environ.* **2005**, *59*, 91–98.
34. Alvarez-Lemus, M.; López, T.; Recillas, S.; Frías, D.M.; Montes, M.; Delgado, J.J.; Centeno, M.A.; Odriozola, J.A. Photocatalytic degradation of 2, dichlorophenoxyacetic acid using nanocrystalline cryptomelane composite catalysts. *J. Mol. Catal. A Chem.* **2008**, *281*, 107–112.

35. Liu, G.; Liao, S.; Zhu, D.; Cui, J.; Zhou, W. Solid-phase photocatalytic degradation of polyethylene film with manganese oxide. *Solid State Sci.* **2011**, *46*, 1290–1295.
36. Yeung, K.L.; Yau, S.T.; Maira, A.J.; Coronado, J.M.; Soria, J.; Yue, P.L. The influence of surface properties on photocatalytic activity of nanostructured TiO<sub>2</sub>. *J. Catal.* **2003**, *219*, 107–116.
37. Lu, X.; Song, C.; Jia, S.; Tong, Z.; Tang, X.; Teng, Y. Low-temperature selective catalytic reduction of NO<sub>x</sub> with NH<sub>3</sub> over cerium and manganese oxides supported on TiO<sub>2</sub>-graphene. *Chem. Eng. J.* **2015**, *260*, 776–784.
38. Huang, Y.; Ho, W.; Lee, S.; Zhang, L.; Li, G.; Jimmy, C.Y. Effect of carbon doping on the mesoporous structure of nanocrystalline tita-nium dioxide and its solar-light-driven photocatalytic degradation of NO<sub>x</sub>. *Langmuir* **2008**, *24*, 3510–3516.
39. Yu, J.G.; Yu, J.C.; Leung, M.K.P.; Ho, W.K.; Cheng, B.; Zhao, X.J.; Zhao, J.C. Effects of acidic and basic hydrolysis catalysts on the photocatalytic activity and microstructures of bimodal mesoporous titania. *J. Catal.* **2003**, *217*, 69–78.
40. Sun, H.; Bai, Y.; Liu, H.; Jin, W.; Xu, N.; Chen, G.; Xu, B. Mechanism of nitrogen-concentration dependence on pH value: Experimental and theoretical studies on nitrogen-doped TiO<sub>2</sub>. *J. Phys. Chem.* **2008**, *112*, 13304–13309.
41. Zhang, F.; Zhao, J.; Shen, T.; Hidaka, H.; Pelizzetti, E.; Serpone, N. TiO<sub>2</sub>-assisted photodegradation of dye pollutants II. Adsorption and degradation kinetics of eosin in TiO<sub>2</sub> dispersions under visible light irradiation. *Appl. Catal. B Environ.* **1998**, *15*, 147–156.

© 2014 by the authors; licensee MDPI, Basel, Switzerland. This article is an open access article distributed under the terms and conditions of the Creative Commons Attribution license (<http://creativecommons.org/licenses/by/4.0/>).